



Cite this: DOI: 10.1039/d6sc01402j

All publication charges for this article have been paid for by the Royal Society of Chemistry

Using xenon difluoride and 2 Li[Al{OC(CF₃)₃]₄] as an oxidant: from organoxenonium intermediates to (fluoro-)biphenyl radical cations

Konstantin Kloiber,^a Tim Heizmann,^a Benoît Lacombe,^a Philipp Thielert,^{b,c} Malte Sellin,^a Tim Schwandt,^a Sabine Richert,^{b,c} Stefan Weber^b and Ingo Krossing^{a*}

The feasibility of employing the XeF₂/2Li[Al(OR^F)₄] (OR^F = OC(CF₃)₃) system as a deelectronator, formally generating Xe_(g) + 2LiF_(s) + 2□⁺, was investigated. While this proved successful for substrates like ferrocene and 9,10-dichlorooctafluoroanthracene, the system was found to react with the solvents benzene, fluorobenzene (FB) and 1,2-difluorobenzene (2FB). The reaction led to the formation of biphenyl radical cations as arene coupling products. In contrast, the reaction with 1,2,3-trifluorobenzene (3FB) allowed the observation of a persistent organoxenonium ion. Low-temperature NMR control reactions and quantum chemical calculations suggest a xenonium-mediated coupling reaction with organoxenonium ions as intermediates. As a reference for the organoxenonium ions proposed, the perfluorinated tight ion-pair (C₆F₅)Xe-F-Al(OR^F)₃ and the salt [C₆F₅Xe][F{Al(OR^F)₃]₂ were synthesized to assess their stability in combination with the alkoxyaluminate anions used in this work. Oxidation studies showed pronounced solvent effects, with strong oxidation observed in pentafluorobenzene, while in MeCN, ferrocene was found to be oxidized already by XeF₂ alone. These findings not only expand the synthetic utility of XeF₂-based oxidation systems but also provide new insight into the reactivity of organoxenonium ions, contributing to the growing understanding of the role of xenon chemistry in selective oxidative transformations.

Received 17th February 2026

Accepted 27th April 2026

DOI: 10.1039/d6sc01402j

rsc.li/chemical-science

Introduction

The development of high potential oxidants has experienced renewed interest over the past decade, particularly by combination of oxidant cations with weakly coordinating anions (WCAs).^{1–8} The availability of robust WCAs, e.g. [Al(OR^F)₄][–], [(R^FO)₃Al-F-Al(OR^F)₃][–] (OR^F = OC(CF₃)₃), [Al(OTeF₅)₄][–] or [(C₆F₅)₃B-CN-B(C₆F₅)₃][–], enables the stabilization of highly reactive cations and allows redox potentials to be shifted to increasingly positive values.^{9–12} Very recently, this field has been expanded by the development of new aluminum-based Lewis superacids and related weakly coordinating anions derived from organotellurium ligands.¹³ Two general strategies are commonly employed to access reactive cations stabilized by WCAs: (1) metathesis reactions by using for example Li⁺, Ag⁺ or [CPh₃]⁺ salts for halide abstraction,^{8,12,14,15} and (2) direct

oxidation of the substrate with a high potential WCA-oxidant salt (=Ox[WCA]).^{4,7,14,16,17} Here, inorganic reagents such as NO [Al(OR^F)₄], Cu[Al(OR^F)₄] or Ag[Al(OR^F)₄] are readily accessible through a simple metathesis reaction from the corresponding (even commercial)¹⁸ lithium salt and reach very high (solvent-dependent) oxidation potentials up to 1.52 V (NO⁺; 4FB = 1,2,3,4-F₄C₆H₂) and 1.50 V (Cu⁺, Ag⁺, 5FB = C₆F₅H) vs. ferrocene/ferrocenium (Fc⁺⁰).^{15,19–21} Notably, borate-WCAs such as [B(C₆F₅)₄][–] or [B(3,5-C₆H₃(CF₃)₂)₄][–] anodically oxidize already at moderate potentials to give fluorinated biphenyls electrochemically in good yields, showcasing their limited stability at higher potentials.²² In addition, the solvent-free Ag [B(C₆F₅)₄] decomposes to AgC₆F₅ and B(C₆F₅)₃.²³ Furthermore, although classical WCAs such as [MF₆][–] (P, Sb, As) have high electrochemical stability, they tend to induce low solubilities and anion coordination in organic media; the latter is often followed by fluoride ion abstraction.^{24–26}

Yet, despite the fact that inorganic oxidants paired with excellent WCAs have enabled the isolation and study of novel reactive species and unusual oxidation states throughout the periodic system,^{2,5,7,27–29} reagents with NO⁺, Cu⁺, Ag⁺ or related active cations are limited by two major challenges:^{30,31} first, their redox potential is strongly influenced by the solvent and environment, and second, the cations tend to undergo side

^aInstitute of Inorganic and Analytical Chemistry, Freiburg Materials Research Center (FMF), University of Freiburg, Albertstr. 21, 79104 Freiburg, Germany. E-mail: krossing@uni-freiburg.de

^bInstitute of Physical Chemistry, University of Freiburg, Albertstr. 21, 79104 Freiburg, Germany

^cInstitute of Physical Chemistry II, University of Ulm, Lise-Meitner-Str. 16, 89081 Ulm, Germany



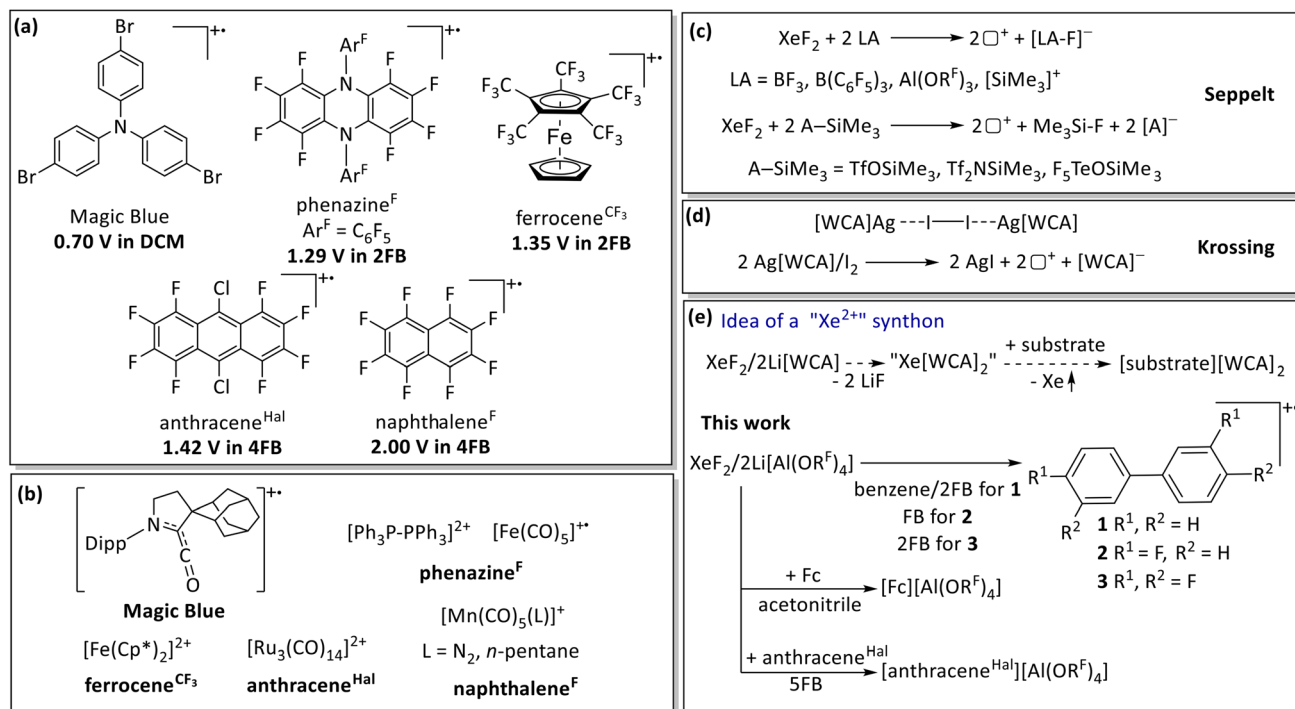


Fig. 1 Selected examples for (a) selective deelectronators including their half wave potential given vs. Fc⁺⁰ and (b) some selected applications to prepare unusual compounds in synthetic chemistry.^{4,17,32–34,42–46} The generated cation is shown in regular font with summary or structural formula and the deelectronator reagents in bold using the abbreviation defined in (a). Cp* = C₅Me₅; Dipp = 2,6-*i*-Pr₂-C₆H₃. (c) Application of XeF₂ as an oxidizing system in combination with Lewis acids (LA = BF₃, B(C₆F₅)₃, Al(OR^F)₃) or silylated derivatives of strong Brønsted acids (A-SiMe₃ = TfOSiMe₃, Tf₂NSiMe₃, F₅TeOSiMe₃).³ (d) The oxidative system 2Ag[Al(OR^F)₄]/I₂.⁴⁷ (e) This work: investigation of the oxidative system XeF₂/2Li[Al(OR^F)₄] with different (fluorinated) arenes and evaluation of its oxidative potential in acetonitrile and 5FB (anthracene^{Hal} = 9,10-dichlorooctafluoroanthracene).

reactions by forming complexes with the substrate (*e.g.* Ag⁺ and Fe(CO)₅) or undergoing ligand substitution (*e.g.*, NO⁺ and Fe(CO)₅).^{13,17,28,29} Consequently, alternative oxidants have been developed in recent years to address these limitations. They act as selective deelectronators that do not react with the substrates through further bond-breaking and bond-making processes (Fig. 1a). With such reagents in hand, we and others were able to access new highly reactive species, *e.g.*, the [Fe(CO)₅]⁺ metalloradical or the [Ph₃P-PPh₃]²⁺ dication (Fig. 1b).^{4,17,32–34}

In this realm, XeF₂ is known as a versatile reagent with strong oxidizing and fluorinating properties and, unlike higher xenon fluorides, is kinetically stable and comparatively easy to handle, which has made it a widely used reagent in synthesis.³⁵ In the presence of strong fluoride acceptors or Lewis acids, XeF₂ can be converted into highly reactive and strongly oxidizing systems that are commonly rationalized in terms of fluoride abstraction and [XeF]⁺-type reactivity.^{36–38} In particular, combinations of XeF₂ with strong Lewis acids such as BF₃ and B(C₆F₅)₃, or Lewis superacids such as Al(OR^F)₃, have been shown to display markedly enhanced reactivity, ranging from electrophilic fluorination/dearomatization of fluoroarenes to oxidation of suitable substrates, depending on the reaction partner and medium (Fig. 1c).^{3,37–41}

Building on this chemistry, the present study explores the "activation" of XeF₂ by a combination of two equivalents of Li

[Al(OR^F)₄] as an oxidizing system. In analogy to the known XeF₂/2LA and the closely related 2Ag[WCA]/I₂ systems (Fig. 1c and d), our approach aims to exploit the formally possible 2e⁻ redox capabilities of the system XeF₂ + 2Li⁺ → "Xe²⁺" + 2LiF → Xe_(g) + 2LiF_(s) + 2□⁺ (□⁺ = positive hole) by utilizing the thermodynamic driving forces of the formation of Xe gas and stable solid LiF (Δ_{latt}H = 1030 kJ mol⁻¹, Fig. 1e).⁴⁸ Here, we found the XeF₂/2Li[Al(OR^F)₄] system to act as a deelectronator for simple substrates like Fc⁰, but also delocalized high potential systems like anthracene^{Hal} (1.42 V vs. Fc⁺⁰) in MeCN or 5FB solution (Fig. 1a). This already underpins that the system reacts with the somewhat less oxidation stable solvents fluorobenzene (FB) and 1,2-difluorobenzene (2FB) to form biphenyl radical cations as arene coupling products. In contrast, 1,2,3-trifluorobenzene (3FB) does not yield radical cations but instead allows observation of a persistent organoxenonium ion. The mechanism of arene coupling and the stability of the involved organoxenonium ions were investigated.

Results and discussion

Initial observations

To investigate whether commercially available Li[Al(OR^F)₄] can serve to activate XeF₂ as a potential two-electron oxidant, the reaction of XeF₂ with two equivalents of Li[Al(OR^F)₄] in



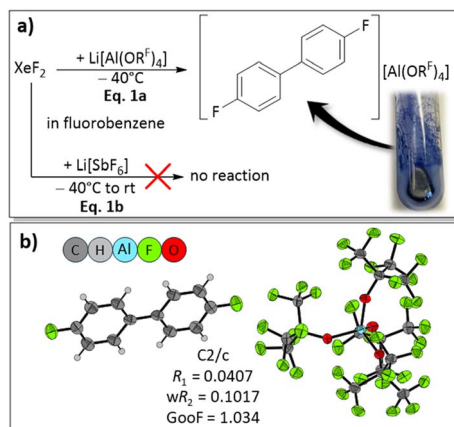


Fig. 2 (a) Overall reaction scheme for the reaction of XeF_2 with $\text{Li}[\text{Al}(\text{OR}^{\text{F}})_4]$ in fluorobenzene leading to blue crystals of [4,4'-difluorobiphenyl][$\text{Al}(\text{OR}^{\text{F}})_4$]. In contrast, no reaction was observed when $\text{Li}[\text{SbF}_6]$ was used under these conditions, including a room temperature reaction. (b) Molecular structure of [4,4'-difluorobiphenyl][$\text{Al}(\text{OR}^{\text{F}})_4$]. Thermal displacement ellipsoids are shown at a 50% probability level.

fluorobenzene (FB) was chosen as a starting point. Immediately after XeF_2 was added to the $\text{Li}[\text{Al}(\text{OR}^{\text{F}})_4]$ solution, the reaction mixture turned intensely blue, potentially indicating the formation of radicals (Fig. 2a, eqn (1a)).⁴⁹ The remarkable speed in color change suggested that the lithium salt of the alkoxaluminates is a promising source for XeF_2 activation. In contrast, the analogous reaction employing $\text{Li}[\text{SbF}_6]$ resulted in no observable changes, neither at -40°C nor at room temperature (Fig. 2a). This is probably caused by the high lattice energy of $\text{Li}[\text{SbF}_6]$ and therefore its poor solubility in FB. When the deep blue reaction mixture resulting from reaction with $\text{Li}[\text{Al}(\text{OR}^{\text{F}})_4]$ was layered with *n*-pentane and stored at -35°C , some blue crystals of [4,4'-difluorobiphenyl][$\text{Al}(\text{OR}^{\text{F}})_4$] suitable for scXRD were isolated (scXRD = single crystal X-ray diffraction; Fig. 2b). Triggered by this observation, the reaction was investigated in more depth.

Scope of the reaction and characterization

To investigate the generality of the reaction in Fig. 2a, the system $\text{XeF}_2/2\text{Li}[\text{Al}(\text{OR}^{\text{F}})_4]$ was also used in combination with a mixture of benzene in 1,2-difluorobenzene (2FB) and in pure 2FB. The reaction of $\text{XeF}_2/2\text{Li}[\text{Al}(\text{OR}^{\text{F}})_4]$ with benzene/2FB led to an intensely yellow colored solution, while the system in 2FB also had an intense blue color. After quenching these reactions by adding H_2O and stirring under atmospheric conditions, followed by work up including purification by column chromatography (Silica 60/*n*-pentane), the neutral species biphenyl (1, bb), 4,4'-difluorobiphenyl (2, fbfb) and 3,3',4,4'-tetrafluorobiphenyl (3, 2fb2fb) were isolated and characterized by NMR spectroscopy.

EPR analyses were performed on the intensely colored solutions, leading after work up to 1–3. The simulations of the EPR spectra agree with their assignment as the radical cations $[1]^{\bullet+}$, $[2]^{\bullet+}$ and $[3]^{\bullet+}$ (see Fig. 3) and prove the formation of the radical cations in Scheme 1.

In contrast to the three reactions of benzene, FB and 2FB, the reaction of 1,2,3-trifluorobenzene (3FB) in 5FB proceeds more slowly and is accompanied by a color change of the solution to brown. In the EPR spectrum of the reaction mixture, no paramagnetic species were detected. Low-temperature NMR analysis of the reaction mixture revealed several fluorinated arenes in the ^{19}F NMR spectrum, including a species identified as the organoxenonium ion $[2,3,4\text{-C}_6\text{H}_2\text{F}_3\text{Xe}]^+$ (see Fig. 4). Remarkably, this species could also be observed at room temperature. Note that two factors likely contribute to the stability of xenonium ions in the present case: (1) stabilization by the electron-withdrawing effect of the fluorine substituents in the *ortho*- and *para*-position and (2) for *ortho*-fluorinated substrates, an additional fluorine-xenon interaction/chelate effect.⁴⁹ Both likely account for the stability of this xenonium ion. Apparently, the enhanced stability of the observed xenonium ion and the low reactivity of the π -system of 3FB are the reasons why the reaction stops at this stage (see below, Scheme 5, proposed mechanism, step C). However, common side reactions of excess

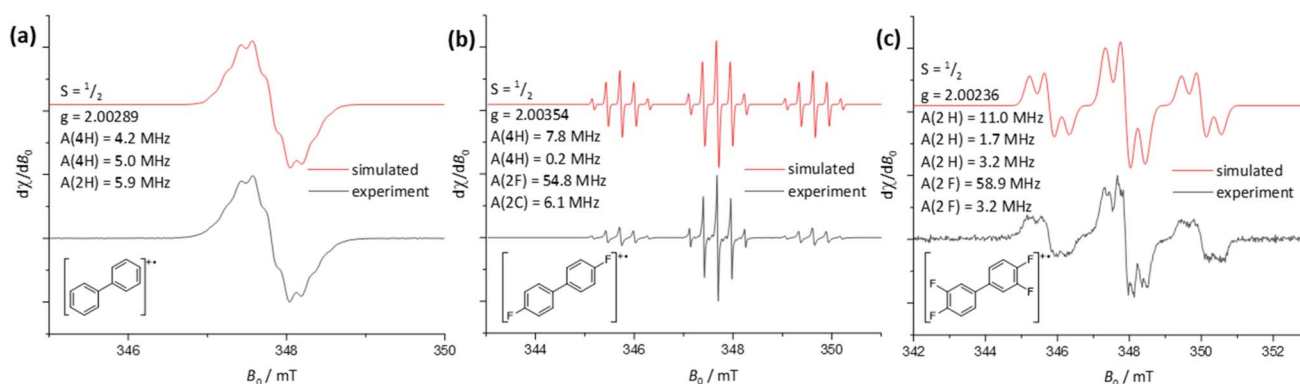
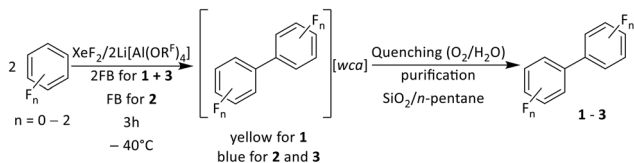


Fig. 3 Continuous wave EPR spectra of the reaction solutions of $\text{XeF}_2/2\text{Li}[\text{Al}(\text{OR}^{\text{F}})_4]$ with (a) benzene in 2FB, (b) FB and (c) 2FB. All reactions were performed at -40°C . The resulting deep yellow (a) or deep blue (b + c) reaction solutions were transferred to EPR tubes under an inert atmosphere and subsequently measured at room temperature.





Scheme 1 Reaction of $\text{XeF}_2/2\text{Li}[\text{Al}(\text{OR}^{\text{F}})_4]$ with benzene, fluoro-benzene (FB) and 1,2-difluorobenzene (2FB) yielding the homocoupling products biphenyl (1, bb), 4,4'-difluorobiphenyl (2, fbfb) and 3,3',4,4'-tetrafluorobiphenyl (3, 2fb2fb), respectively. In the initial step, one equivalent of $\text{XeF}_2/2\text{Li}[\text{Al}(\text{OR}^{\text{F}})_4]$ leads to the neutral coupling product and another equivalent of $\text{XeF}_2/2\text{Li}[\text{Al}(\text{OR}^{\text{F}})_4]$ generates the radical cations of the coupling product. The work up includes stirring the reaction mixtures under atmospheric conditions and purification of 1, 2 and 3 by column chromatography.

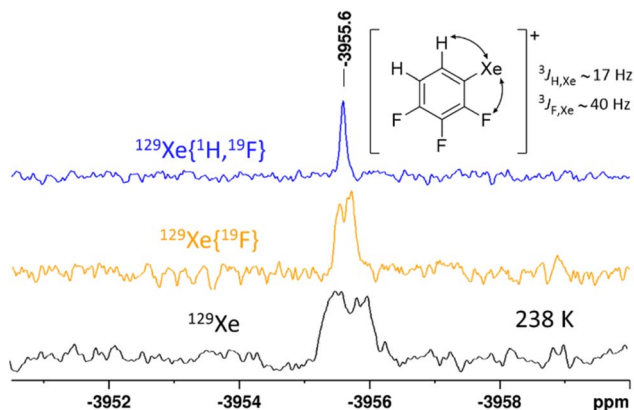
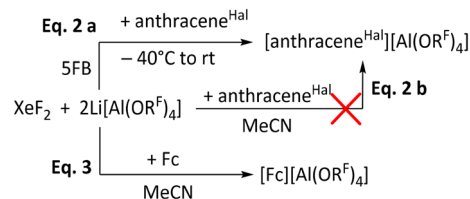


Fig. 4 ^{129}Xe NMR spectra (111.29 MHz) of the reaction $\text{XeF}_2/2\text{Li}[\text{Al}(\text{OR}^{\text{F}})_4]$ in a fluorinated benzene solvent mixture (3FB/5FB) at 238 K. The signal of the observed organoxenonium ion $[\text{C}_6\text{F}_5\text{H}_2\text{Xe}]^+$ is shown in three different decoupling schemes: ^{129}Xe in black, $^{129}\text{Xe}\{^{19}\text{F}\}$ in yellow and $^{129}\text{Xe}\{^1\text{H}, ^{19}\text{F}\}$ in blue. All coupling constants shown here have an uncertainty of 2–3 Hz.

XeF_2 , such as the fluorination of arenes, predominate under these conditions.⁵⁰

Stability of $\text{XeF}_2/2\text{Li}[\text{Al}(\text{OR}^{\text{F}})_4]$ and its potential

After establishing that $\text{XeF}_2/2\text{Li}[\text{Al}(\text{OR}^{\text{F}})_4]$ induces coupling of lower fluorinated arenes, like FB and 2FB, the system was investigated using 5FB as solvent, which has the highest published positive electrochemical solvent limit of all fluorobenzenes of +2.67 V vs. $\text{Fc}^{+/0}$.¹⁹ XeF_2 alone was found to be stable at room temperature for up to two hours, after which fluorination of 5FB was observed (SI 4.1). Subsequently, the mixture of XeF_2 and $2\text{Li}[\text{Al}(\text{OR}^{\text{F}})_4]$ was analyzed by NMR spectroscopy at -35°C . This analysis revealed that similar fluorination reactions occur rapidly in this mixture even at low temperatures. Therefore, the addition of XeF_2 to a solution of $\text{Li}[\text{Al}(\text{OR}^{\text{F}})_4]$ in the presence of a redox active substrate appeared as a logical consequence to estimate its potential. For this purpose, 9,10-dichlorooctafluoroanthracene (anthracene^{Hal}) was selected.



Scheme 2 Tests on the oxidation potential of $\text{XeF}_2/2\text{Li}[\text{Al}(\text{OR}^{\text{F}})_4]$: oxidation of anthracene^{Hal} (=9,10-dichlorooctafluoro-anthracene) to $[\text{anthracene}^{\text{Hal}}][\text{Al}(\text{OR}^{\text{F}})_4]$ in 5FB, but not in acetonitrile. In contrast, ferrocene is already oxidized in MeCN by XeF_2 alone and $\text{Li}[\text{Al}(\text{OR}^{\text{F}})_4]$ acts as a metathesis reagent affording $\text{Fc}[\text{Al}(\text{OR}^{\text{F}})_4]$.

Upon adding XeF_2 and gradual warming to rt, a color change to deep green took place, characteristic of the radical cation $[\text{anthracene}^{\text{Hal}}]^{\cdot+}$ (Scheme 2). This indicates that $\text{XeF}_2/2\text{Li}[\text{Al}(\text{OR}^{\text{F}})_4]$ in 5FB reaches a potential of at least 1.42 V vs. $\text{Fc}^{+/0}$.³² In addition to 5FB, acetonitrile was also considered as a potential solvent. The observed stability of XeF_2 in acetonitrile under the present conditions is consistent with previous literature reports, and XeF_2 was found to remain stable for several days in this solvent (SI 4.2).⁵¹ While $\text{XeF}_2/2\text{Li}[\text{Al}(\text{OR}^{\text{F}})_4]$ can oxidize Fc in acetonitrile, anthracene^{Hal} could not be oxidized in this solvent (Scheme 2). Notably, control experiments demonstrated that Fc can already be oxidized by XeF_2 alone in MeCN, suggesting that $\text{Li}[\text{Al}(\text{OR}^{\text{F}})_4]$ primarily acts as a metathesis reagent to afford $\text{Fc}[\text{Al}(\text{OR}^{\text{F}})_4]$. These findings indicate that the enhanced reactivity of the $\text{Xe}/2\text{Li}[\text{Al}(\text{OR}^{\text{F}})_4]$ system is suppressed in MeCN, likely due to the increased solvation and consequently reduced reactivity of the Li^+ ion in this system.

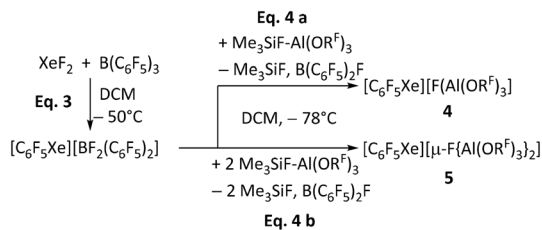
Synthesis of $[\text{C}_6\text{F}_5\text{Xe}]^+$ -compounds and stability with aluminate WCAs

Various counterions have hitherto been used to synthesize and stabilize organoxenonium ions, including tetrafluoroborate and related fluoroborate-derived anions, and more recent work has further broadened the synthetic access to aryxenonium(II) salts.^{49,52–61} However, to date, no examples are reported utilizing perfluorinated alkoxyaluminate anions as WCAs. In combination with the above assignment of the $[\text{2,3,4-C}_6\text{H}_2\text{F}_3\text{Xe}]^+$ intermediate, this raised the question of whether organoxenonium species are compatible with aluminate anions, or if the observed decomposition of the anion is a result of such incompatibility. To address this, we aimed to synthesize salts with the well-established $[\text{C}_6\text{F}_5\text{Xe}]^+$ cation and aluminate-WCAs as the counterion to directly assess their compatibility.

A modified route to $[\text{C}_6\text{F}_5\text{Xe}]^+$ salts

The established synthesis of the organoxenonium ion $[\text{C}_6\text{F}_5\text{Xe}][\text{AsF}_6]$ with the intermediate $[\text{C}_6\text{F}_5\text{Xe}][\text{BF}_2(\text{C}_6\text{F}_5)_2]$ served as the starting point for our route (see Scheme 3).⁵³ To obtain the xenonium compounds, our route uses the “ion-like” trimethylfluorosilane adduct $(\text{CH}_3)_3\text{SiF}-\text{Al}(\text{OR}^{\text{F}})_3$ as a strong Lewis acid (FIA = 459 kJ mol^{-1})^{62,63} to abstract a fluoride ion from $[\text{BF}_2(\text{C}_6\text{F}_5)_2]^-$. Depending on the number of equivalents of





Scheme 3 Synthesis of the compounds [C₆F₅Xe][WCA] ([WCA]⁻ = [FAl(OR^F)₃]⁻ (4), [μ-FAl(OR^F)₃]₂⁻ (5)) starting from the established synthesis of [C₆F₅Xe][BF₂(C₆F₅)₂] by Frohn *et al.*⁵³

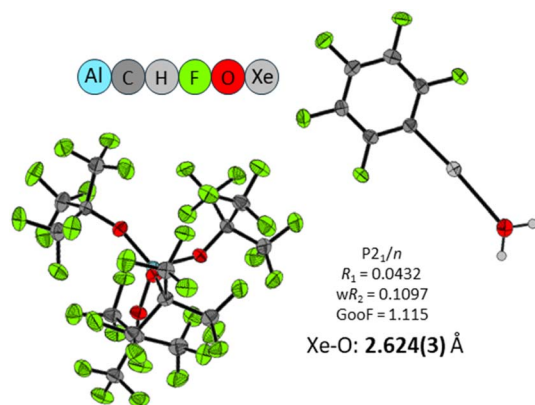


Fig. 5 Molecular structures of [C₆F₅Xe(H₂O)][Al(OR^F)₄]. Selected bond length: Xe⋯O(H₂O) = 2.624(3) Å. Thermal displacement ellipsoids are shown at the 50% probability level.

Me₃SiF-Al(OR^F)₃ employed, we successfully synthesized [C₆F₅Xe][WCA] ([WCA]⁻ = [FAl(OR^F)₃]⁻ (4), [μ-FAl(OR^F)₃]₂⁻ (5), see Scheme 3). Both compounds 4 and 5 were characterized by NMR, IR and scXRD (SI 5.7, 5.8, 8.2 and 9).

During these investigations, crystals of [C₆F₅Xe(OH₂)][Al(OR^F)₄] were obtained accidentally when Li[Al(OR^F)₄] was used instead of Me₃SiF-Al(OR^F)₃ (SI 8.3). While characterized only by scXRD, this species constitutes a rare structural example of a xenonium water complex (Fig. 5). The short Xe⋯O(H₂O) contact of 2.624(3) Å supports coordination of water to the xenonium center. For comparison, recently characterized Xe(vi) hydrate complexes exhibit similarly short Xe⋯O(H₂O) contacts, *e.g.* in [(18-crown-6)(H₂O)XeO₃]·H₂O, the corresponding Xe⋯O(H₂O) distance is 2.702(10) Å. However, the bonding situation in the present organoxenonium species is clearly different from that in XeO₃.⁶⁴

Molecular structures

The molecular structure of the xenonium ion [C₆F₅Xe]⁺ shows distinct interactions depending on the counterion. With the anion [F-Al(OR^F)₃]⁻, the compound crystallizes in the orthorhombic space group *Pbca*, forming a contact ion pair. The shortest Xe⋯F(Al) contact is 2.595 Å, notably shorter than the 2.714 Å observed in [C₆F₅Xe][AsF₆],⁵³ indicating a stronger cation-anion interaction in the tetrahedral, monodentate anion [F-Al(OR^F)₃]⁻. By contrast, when the least coordinating WCA [μ-FAl(OR^F)₃]₂⁻ is employed,¹² the salt [C₆F₅Xe][μ-FAl(OR^F)₃]₂ crystallizes in the monoclinic space group *P2₁/n*, and the closest Xe⋯F contact increases to 2.981 Å. This expanded distance reflects the much weaker interaction, yielding a nearly “naked” xenonium species that better represents the intrinsic properties of the isolated [C₆F₅Xe]⁺ cation. These structural differences demonstrate how the anion's coordination behavior and fluorine bridging capacity modulate cation-anion interactions.

The Hirshfeld surface analysis of the scXRD structures of [C₆F₅Xe][FAl(OR^F)₃]₂ and C₆F₅Xe-F-Al(OR^F)₃ clearly

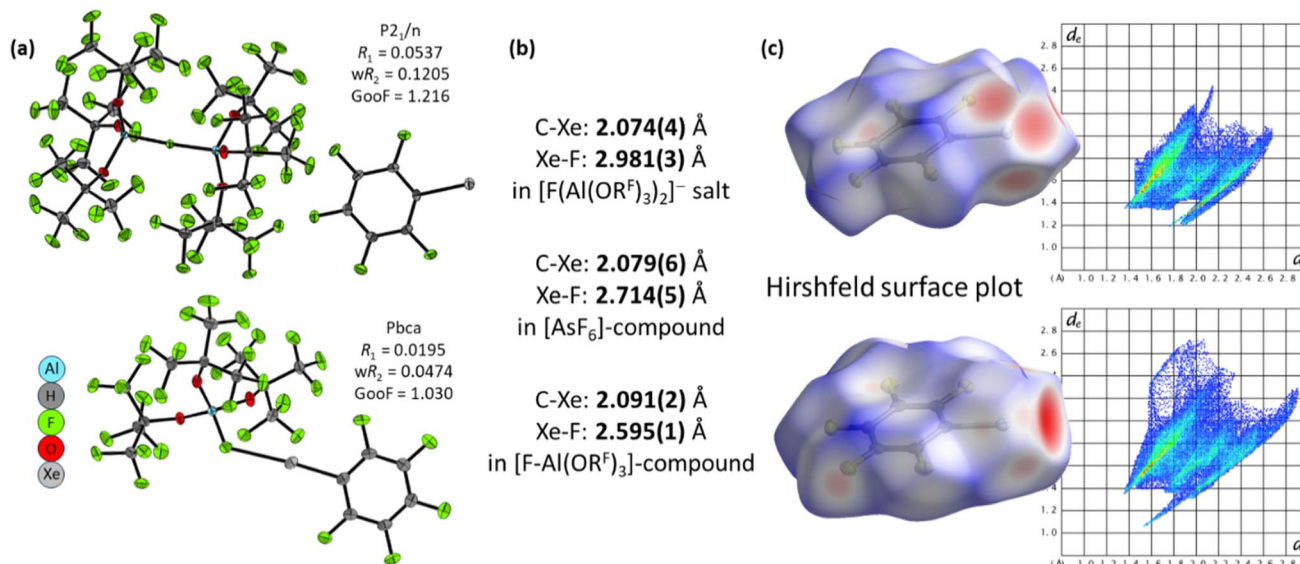
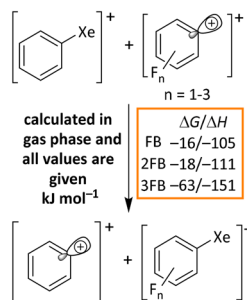


Fig. 6 Overview of (a) molecular structures of [C₆F₅Xe][FAl(OR^F)₃]₂ and [C₆F₅Xe-μ-F-Al(OR^F)₃], (b) selected bond lengths with corresponding values in the [AsF₆]⁻ compound for reference, and (c) Hirshfeld surface plot illustrating the interaction with the counterion. Thermal displacement ellipsoids are shown at the 50% probability level. Hirshfeld surfaces were calculated and mapped with *d*_{norm} for visualizing close contacts and intermolecular interactions (-0.57 (red)-1.24 (blue)), including their corresponding fingerprint plots.





Scheme 4 Calculated ΔG and ΔH values (kJ mol^{-1}) for a Xe-atom exchange between $[\text{C}_6\text{H}_5\text{Xe}]^+$ and fluorinated phenyl cations in the gas phase using the $r^2\text{scan-3c}$ functional with D4 dispersion correction in combination with the def2-mTZVPP basis set.

demonstrates the stronger interaction of the $[\text{FAl}(\text{OR}^{\text{F}})_3]^-$ anion with the cation (see Fig. 6c). On the Hirshfeld surface, the red regions correspond to contacts that are shorter than the sum of the van der Waals radii, indicating enhanced intermolecular interactions.

Stability of arene-xenonium ions

To revisit the literature statement that xenonium species derived from highly fluorinated arenes exhibit increased stability with rising degrees of fluorination⁶⁵ and to support the stability of the observed 2,3,4-trifluorophenylxenonium ion, this trend was quantified by density functional theory (DFT) calculations (RI- $r^2\text{scan-3c(D4)/def2-mTZVPP}$) by investigating the isodesmic transfer of a xenon atom from a phenyl xenonium ion onto a fluorinated phenyl cation: Scheme 4 shows that the reaction turns increasingly exergonic as the degree of fluorination increases.

Proposed mechanism for biphenyl-formation and quantum chemical calculations

With this knowledge in mind, we now turn to the question of what mechanism leads to the observed radical cations of the coupling products $[1]^+$, $[2]^+$ and $[3]^+$. Filler *et al.* proposed that the coupling of arenes induced by XeF_2 in the presence of HF proceeds *via* a radical mechanism, involving the formation of the phenyl radical as a key intermediate, since no other intermediates were observed that could support an electrophilic mechanism.⁶⁶ However, in the present $\text{XeF}_2/2\text{Li}[\text{Al}(\text{OR}^{\text{F}})_4]$ system, we observe the concomitant formation of $\text{Li}[\text{FAl}(\text{OR}^{\text{F}})_3]$ and HOR^{F} , as well as in the low-temperature NMR studies the development of the 2,3,4-trifluorophenylxenonium ion. Therefore, we propose the electrophilic aromatic substitution mechanism shown in Scheme 5, based on experimental evidence that is further supported by DFT calculations in the subsequent section.

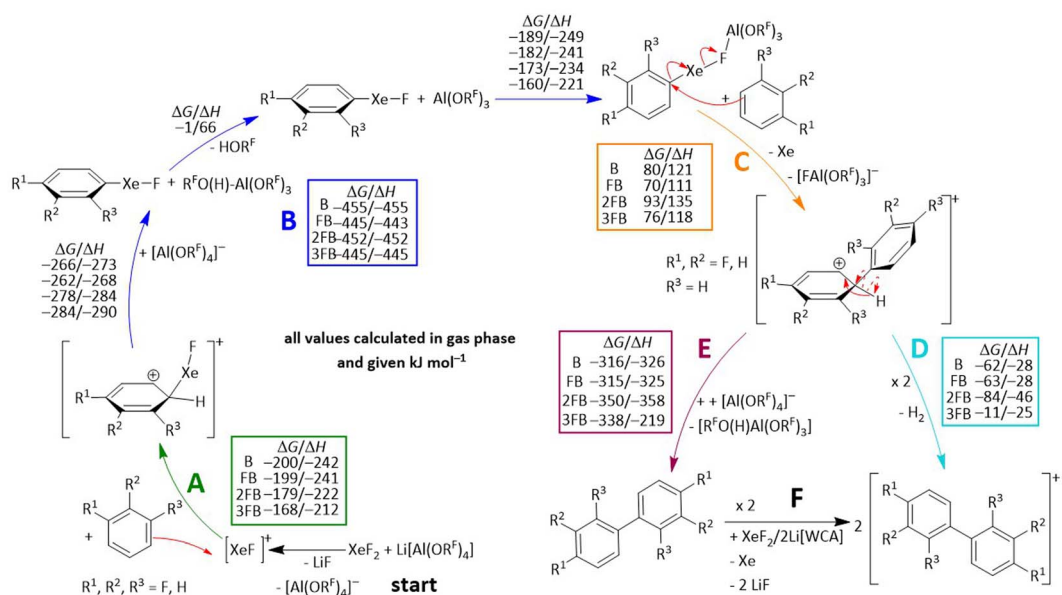
Organoxenonium-ion formation

The hypothetical mechanism begins with the formation of LiF and $[\text{XeF}][\text{Al}(\text{OR}^{\text{F}})_4]$ in a medium that weakly solvates Li^+ . The xenonium species generated then acts as a strong electrophile and forms Wheland intermediates with the arenes benzene, FB, 2FB and 3FB (step A in Scheme 5). The +M-effect of the fluorine substituent accounts for the observed substitution patterns in the products. While formal elimination of HF from this Wheland intermediate could in principle yield the organoxenonium species directly, we presume instead that this intermediate reacts as a very strong Brønsted acid by protonation of one of the oxygen atoms of a second equivalent of the counterion $[\text{Al}(\text{OR}^{\text{F}})_4]^-$ yielding the known, but weakly bound alcohol adduct $\text{R}^{\text{F}}\text{O}(\text{H})-\text{Al}(\text{OR}^{\text{F}})_3$. The latter dissociates into the corresponding alcohol as well as the known Lewis super acid $\text{Al}(\text{OR}^{\text{F}})_3$.⁶⁷ The Lewis super acid then abstracts in step B a fluoride ion from the Xe-compound to probably generate a contact ion pair, related to the independently prepared $[\text{C}_6\text{F}_5\text{Xe}-\mu\text{-F-Al}(\text{OR}^{\text{F}})_3]$. Subsequently, the organoxenonium species acts as a $[\text{CH}_{5-n}\text{F}_n]^+$ ($n = 0-3$) phenyl cation synthon and undergoes coupling with a second equivalent of the arene, accompanied by liberation of neutral xenon gas, to yield the coupling product in step C, again viewed as being formally a protonated (fluorinated) biphenyl $[\text{H}(\text{CH}_{5-n}\text{F}_n)_2]^+$ and thus a very strong Brønsted acid. For the final step, two mechanistic pathways are conceivable (D and E). Pathway D would directly lead to the observed radical cation coupling products *via* the formal elimination of a hydrogen atom (resulting in H_2 evolution). Although this step is calculated to be exergonic, such a reaction is highly unusual. Notably, literature examples exist for protonated arenes, *e.g.* $[\text{H}(\text{mesitylene})]^+$,⁶⁸ yet in those cases the formation of the corresponding radical cation was never reported. Instead, we assume that the deprotonation of this species, followed by rearomatization, takes place, which yields the neutral coupling products in step E. As Poleschner *et al.* have demonstrated, the combination of XeF_2 with the Lewis acid $\text{Al}(\text{OR}^{\text{F}})_3$ acts as a strongly oxidizing system.³ However, the identity of the final oxidant remains ambiguous, as both XeF_2 in combination with the Lewis acid and $\text{Li}[\text{Al}(\text{OR}^{\text{F}})_4]$ could account for the formation of the observed radical cations of the coupling products in step G.

DFT calculations

To support the proposed mechanism, we performed DFT calculations to assess the underlying thermodynamics in the gas phase, employing the cost-efficient but accurate D4 dispersion corrected $r^2\text{scan-3c}$ functional with the def2-mTZVPP basis set (Scheme 5).⁶⁹ The first two reaction steps A and B are highly exergonic, which is in line with the experimental observation that the reactions even take place at -40°C . Step C is moderately endergonic for all calculated arenes. Yet, this unfavorable thermodynamics is probably caused by the formation of two charged species from a neutral molecule. Bond heterolysis will be favored by polar solvents and should also be favorable in solution. By comparing steps D and E, the deprotonation and rearomatization are clearly





Scheme 5 Proposed mechanism of the coupling reaction towards the observed biphenyl derivatives. Quantum chemical calculations for each step were performed for the gas phase using the $r^2\text{scan-3c}$ functional with D4 dispersion correction in combination with the def2-mTZVPP basis set. Reaction steps (A, B, D and E) are highly exergonic, which is consistent with the fast reaction observed at -40°C . Moderately endergonic step (C) produces two ions from a neutral molecule and hence will profit from the polar reaction medium, presumably tipping it to exergonic reaction progress. For the final step, deprotonation and rearomatization (E) are more likely than formal H-radical and then H_2 formation (D), which would directly generate the observed radical cation of the coupling product.

thermodynamically favored, which underlines the assumption of forming the neutral coupling product followed by oxidation of another equivalent of $\text{XeF}_2/2\text{Li}[\text{Al}(\text{OR}^F)_4]$. For benchmarking the protonation steps B and D, we also calculated the reaction $[\text{H}(\text{mesitylene})]^+ + [\text{Al}(\text{OR}^F)_4]^- \rightarrow \text{mesitylene} + \text{R}^F\text{O}(\text{H})-\text{Al}(\text{OR}^F)_3$, which exhibits gaseous $\Delta G/\Delta H$ values of $-216/-223 \text{ kJ mol}^{-1}$ (RI- $r^2\text{scan-3c(D4)/def2-mTZVPP}$). Note that $[\text{H}(\text{mesitylene})]^+[\text{Al}(\text{OR}^F)_4]^-$ is experimentally known to be stable in DCM solution at -20°C , but decomposes slowly over hours at RT.⁶⁷ This comparison is particularly relevant, since both reactants are charged and the products are neutral, like steps B and D in the proposed mechanism. However, both steps are considerably more exergonic than this reference reaction, further supporting the conclusion that anion protonation is also favorable in solution.

Overall, experiments and calculations support the conclusion that the $\text{XeF}_2/2\text{Li}[\text{Al}(\text{OR}^F)_4]$ system mediates the coupling of arenes, followed by oxidation of the resulting biphenyl derivatives.

Conclusion

Through the combination of XeF_2 and $\text{Li}[\text{Al}(\text{OR}^F)_4]$ in polar but almost non-coordinating fluorobenzene solvents, activation of XeF_2 was achieved at low temperature. With benzene (dissolved in 2FB), FB and 2FB, this led to coupling reactions forming the biphenyl derivatives 1–3 and their oxidation to the corresponding radical cations. A weakly solvated Li^+ source is essential, as $\text{Li}[\text{SbF}_6]$ showed no reactivity under analogous conditions and acetonitrile blocked reactions in separate

experiments. The observation of the 2,3,4-trifluorophenylxenonium ion using 3FB suggests an electrophilic mechanism, which was further explored through DFT studies. The successful synthesis of compounds 4 and 5 demonstrates the compatibility of organoxenonium species with alkoxy aluminates as anions. Stability studies of XeF_2 at room temperature revealed that it remains stable for 2 h in 5FB before fluorination of 5FB occurs, whereas in acetonitrile XeF_2 is stable for several days.

By choosing suitable reagents, we showed that the $\text{XeF}_2/2\text{Li}^+$ system can react as an oxidant in suitable and compatible solvents. Upon reaction with anthracene^{Hal} in 5FB, the characteristic intensely green colored solutions of $[\text{anthracene}^{\text{Hal}}]^+$ were formed, indicating a redox potential of the system of at least 1.42 V vs. $\text{Fc}^{+/0}$ in 5FB. In contrast, no oxidation of anthracene^{Hal} was observed in MeCN. Control experiments further showed that Fc can already be oxidized by XeF_2 alone, whereas addition of $\text{Li}[\text{Al}(\text{OR}^F)_4]$ affords $[\text{Fc}][\text{Al}(\text{OR}^F)_4]$. Thus, in acetonitrile, $\text{Li}[\text{Al}(\text{OR}^F)_4]$ appears to mainly act as a metathesis reagent and yields a stable counterion for the ferrocenium cation. This led to the conclusion that the “price” for the higher stability of XeF_2 in acetonitrile is the well solvated and hence less active Li^+ in solution.

In summary, the $\text{XeF}_2/2\text{Li}[\text{Al}(\text{OR}^F)_4]$ system exhibits high reactivity even at low temperatures but is accompanied by challenges due to side reactions. In 5FB, it enables access to high potentials up to 1.42 V and potentially even higher, whereas acetonitrile offers better XeF_2 stability but suppresses the enhanced reactivity of the combined $\text{XeF}_2/2\text{Li}^+$ system. Consequently, side reactions such as arene fluorination or



coupling reactions and restricted solvent choice (favoring 5FB) represent key limitations. The isolated xenonium salts expand the field of xenon chemistry by demonstrating that readily available alkoxyaluminates can serve as anions. In addition, the observation of $[\text{C}_6\text{F}_5\text{Xe}(\text{OH}_2)][\text{Al}(\text{OR}^F)_4]$ provides a rare example of a xenonium water complex. The observed radical cations of fluorinated biphenyls exhibit significant potential as strong oxidants and are the subject of intense ongoing studies.

Author contributions

KK performed the majority of the syntheses and characterizations, carried out the DFT calculations and analyses, and co-wrote the manuscript together with IK. TH synthesized the $[\text{C}_6\text{F}_5\text{Xe}][\text{WCA}]$ species together with MS. BL investigated the coupling products under the supervision of KK. TS synthesized the $[\text{C}_6\text{F}_5\text{Xe}(\text{OH}_2)]^+$ species under the supervision of KK. PT and SR performed the EPR measurements and simulations, and wrote and reviewed the corresponding section of the manuscript. IK conceived and supervised the project.

Conflicts of interest

The authors declare no conflict of interest.

Data availability

CCDC 2529884–2529886 and 2531335 contain the supplementary crystallographic data for this paper.^{70a–d}

Experimental details, procedures, weights, and 1D- and 2D-NMR spectra of the reactions are provided in the supplementary information (SI). Supplementary information: the general synthetic methods and characterization techniques used for this work together with the experimental procedures. Additional figures such as NMR, IR and EPR spectra are presented, as well as the crystallographic data of the isolated salts and details of the quantum chemical calculations. The authors have cited additional references within the SI. See DOI: <https://doi.org/10.1039/d6sc01402j>.

Acknowledgements

The authors acknowledge support by the state of Baden-Württemberg through bwHPC and the DFG through grant number INST 40/575-1 FUGG (JUSTUS 2 cluster). This work was supported by ERC Advanced Grant InnoChem. This work was supported by the Deutsche Forschungsgemeinschaft (DFG, German Research Foundation) – Project number 417643975 (S. Richert). S. Weber thanks the SIBW/DFG for financing magnetic resonance instrumentation that is operated within the MagRes Center of the University of Freiburg. K. Kloiber is grateful for a Manchot PhD fellowship from the “Jürgen Manchot Stiftung”.

References

- M. Lehmann, A. Schulz and A. Villinger, *Angew. Chem., Int. Ed.*, 2009, **48**, 7444–7447.
- Y. Schulte, C. Wölper, S. M. Rupf, M. Malischewski, D. J. SantaLucia, F. Neese, G. Haberhauer and S. Schulz, *Nat. Chem.*, 2024, **16**, 651–657.
- H. Poleschner and K. Seppelt, *Angew. Chem., Int. Ed.*, 2013, **52**, 12838–12842.
- R. Sievers, N. G. Kub, T. Streit, M. Reimann, G. Thiele, M. Kaupp and M. Malischewski, *Angew. Chem., Int. Ed.*, 2025, **64**, e202505783.
- L. Fischer, M. H. Lee, I. Kim, A. Wiesner, K. F. Hoffmann and S. Riedel, *Angew. Chem., Int. Ed.*, 2024, **63**, e202407497.
- R. Sievers, N. G. Kub, T. Streit, S. M. Rupf and M. Malischewski, *Chem.–Eur. J.*, 2025, **31**, e202500743.
- A. N. Toraman, L. Fischer, A. Pérez-Bitrián, A. Wiesner, K. F. Hoffmann and S. Riedel, *Chem. Commun.*, 2024, **60**, 1711–1714.
- K. F. Hoffmann, D. Battke, P. Golz, S. M. Rupf, M. Malischewski and S. Riedel, *Angew. Chem., Int. Ed.*, 2022, **61**, e202203777.
- T. He, M. A. Bruening, M. Espinosa and T. Agapie, *Angew. Chem., Int. Ed.*, 2025, **64**, e202417136.
- J. Bader, L. Fischer, K. F. Hoffmann, N. Limberg, A. Millanvois, F. Oesten, A. Pérez-Bitrián, J. Schlögl, A. N. Toraman, D. Wegener, A. Wiesner and S. Riedel, *Chem. Rev.*, 2025, **125**, 9140–9186.
- S. Kotsyuda, A. Wiesner, S. Steinhauer and S. Riedel, *Z. Anorg. Allg. Chem.*, 2021, **647**, 200–203.
- A. Martens, P. Weis, M. C. Krummer, M. Kreuzer, A. Meierhöfer, S. C. Meier, J. Bohnenberger, H. Scherer, I. Riddlestone and I. Krossing, *Chem. Sci.*, 2018, **9**, 7058–7068.
- D. Wegener, N. Limberg, M. Bubenik, A. Pérez-Bitrián, A. Wiesner and S. Riedel, *JACS Au*, 2025, **5**, 3565–3574.
- K. F. Hoffmann, A. Wiesner, N. Subat, S. Steinhauer and S. Riedel, *Z. Anorg. Allg. Chem.*, 2018, **644**, 1344–1348.
- I. Krossing, *Chem.–Eur. J.*, 2001, **7**, 490–502.
- J. J. Davidson, S. O. Gunther, D. W. Leong and O. V. Ozerov, *Dalton Trans.*, 2023, **52**, 16027–16031.
- F. Dankert, S. P. Muhm, C. Nandi, S. Danés, S. Mullassery, P. Herbeck-Engel, B. Morgenstern, R. Weiss, P. Salvador and D. Munz, *J. Am. Chem. Soc.*, 2025, **147**, 15369–15376.
- AB155762|CAS 274933-96-9, https://abcr.com/de_de/ab155762, accessed December 4, 2025.
- C. Armbruster, M. Sellin, M. Seiler, T. Würz, F. Oesten, M. Schmucker, T. Sterbak, J. Fischer, V. Radtke, J. Hunger and I. Krossing, *Nat. Commun.*, 2024, **15**, 6721.
- A. Decken, H. D. B. Jenkins, G. B. Nikiforov and J. Passmore, *Dalton Trans.*, 2004, 2496–2504.
- J. Willrett, M. Sellin, M. Lapersonne, M. Seiler and I. Krossing, *Chem.–Eur. J.*, 2025, **31**, e202501134.
- S. B. Beil, S. Möhle, P. Enders and S. R. Waldvogel, *Chem. Commun.*, 2018, **54**, 6128–6131.
- M. F. Ibad, A. Schulz and A. Villinger, *Organometallics*, 2019, **38**, 1445–1458.
- I.-C. Hwang and K. Seppelt, *Inorg. Chem.*, 2003, **42**, 7116–7122.
- P. Gowik, T. Klapötke and U. Thewalt, *J. Organomet. Chem.*, 1990, **385**, 345–350.



- 26 Y. Nakajima, Y. Shiraishi, T. Tsuchimoto and F. Ozawa, *Chem. Commun.*, 2011, **47**, 6332.
- 27 K. F. Hoffmann, A. Wiesner, C. Müller, S. Steinhauer, H. Beckers, M. Kazim, C. R. Pitts, T. Lectka and S. Riedel, *Nat. Commun.*, 2021, **12**, 5275.
- 28 F. S. T. Khan, A. L. Waldbusser, M. C. Carrasco, H. Pourhadi and S. Hematian, *Dalton Trans.*, 2021, **50**, 7433–7455.
- 29 L. Fischer, M. H. Lee, A. Wiesner, C. Müller and S. Riedel, *Chem. Sci.*, 2025, **16**, 13229–13234.
- 30 M. E. Moussa, M. Fleischmann, G. Balázs, A. V. Virovets, E. Peresykina, P. A. Shelyganov, M. Seidl, S. Reichl and M. Scheer, *Chem.–Eur. J.*, 2021, **27**, 9742–9747.
- 31 J. Bohnenberger, W. Feuerstein, D. Himmel, M. Daub, F. Breher and I. Krossing, *Nat. Commun.*, 2019, **10**, 624.
- 32 M. Sellin, C. Friedmann, M. Mayländer, S. Richert and I. Krossing, *Chem. Sci.*, 2022, **13**, 9147–9158.
- 33 M. Schorpp, T. Heizmann, M. Schmucker, S. Rein, S. Weber and I. Krossing, *Angew. Chem., Int. Ed.*, 2020, **59**, 9453–9459.
- 34 M. Sellin, J. Willrett, D. Röhner, T. Heizmann, J. Fischer, M. Seiler, C. Holzmann, T. A. Engesser, V. Radtke and I. Krossing, *Angew. Chem., Int. Ed.*, 2024, **63**, e202406742.
- 35 M. Tramsek and B. Zemva, *Acta Chim. Slov.*, 2006, **53**, 105–116.
- 36 B. Zemva, A. Jesih, D. H. Templeton, A. Zalkin, A. K. Cheetham and N. Bartlett, *J. Am. Chem. Soc.*, 1987, **109**, 7420–7427.
- 37 H. Kim, D. Mandal, J. K. J. Ng, Z. Qu, S. Grimme and D. W. Stephan, *Chem.–Eur. J.*, 2024, **30**, e202401776.
- 38 S. Stavber and M. Zupan, *J. Org. Chem.*, 1981, **46**, 300–302.
- 39 A. Kraft, N. Trapp, D. Himmel, H. Böhrer, P. Schlüter, H. Scherer and I. Krossing, *Chem.–Eur. J.*, 2012, **18**, 9371–9380.
- 40 L. O. Müller, D. Himmel, J. Stauffer, G. Steinfeld, J. Slattery, G. Santiso-Quiñones, V. Brecht and I. Krossing, *Angew. Chem., Int. Ed.*, 2008, **47**, 7659–7663.
- 41 V. V. Bardin, L. N. Shchegoleva and H. J. Frohn, *J. Fluorine Chem.*, 1996, **77**, 153–159.
- 42 L. Ai, X. Meng, S. Li, C. Zhang, D. Munz and J. Chu, *Angew. Chem., Int. Ed.*, 2025, **64**, e202515888.
- 43 M. Quiroz-Guzman and S. N. Brown, *Acta Crystallogr., Sect. C: Cryst. Struct. Commun.*, 2010, **66**, m171–m173.
- 44 N. G. Connelly and W. E. Geiger, *Chem. Rev.*, 1996, **96**, 877–910.
- 45 J. M. Rall, M. Schorpp, M. Keilwerth, M. Mayländer, C. Friedmann, M. Daub, S. Richert, K. Meyer and I. Krossing, *Angew. Chem., Int. Ed.*, 2022, **61**, e202204080.
- 46 M. Sellin, J. D. Watson, J. Fischer, G. E. Ball, L. D. Field and I. Krossing, *Angew. Chem., Int. Ed.*, 2025, **64**, e202507494.
- 47 P. J. Malinowski, D. Himmel and I. Krossing, *Angew. Chem., Int. Ed.*, 2016, **55**, 9262–9266.
- 48 *CRC handbook of chemistry and physics: a ready-reference book of chemical and physical data*, ed. D. R. Lide, CRC Press, CRC, Taylor & Francis, Boca Raton, Fla., 2006, p. 87, 2006–2007.
- 49 D. Naumann, H. Butler, R. Gnann and W. Tyrra, *Inorg. Chem.*, 1993, **32**, 861–863.
- 50 M. Zupan, J. Iskra and S. Stavber, *J. Org. Chem.*, 1998, **63**, 878–880.
- 51 M. A. Tius, *Tetrahedron*, 1995, **51**, 6605–6634.
- 52 H.-J. Frohn, T. Schroer and G. Henkel, *Angew. Chem., Int. Ed.*, 1999, **38**, 2554–2556.
- 53 H.-J. Frohn, A. Klose, T. Schroer, G. Henkel, V. Buss, D. Opitz and R. Vahrenhorst, *Inorg. Chem.*, 1998, **37**, 4884–4890.
- 54 H. J. Frohn, S. Jakobs and G. Henkel, *Angew. Chem., Int. Ed.*, 1989, **28**, 1506–1507.
- 55 K. Koppe, H.-J. Frohn, H. P. A. Mercier and G. J. Schrobilgen, *Inorg. Chem.*, 2008, **47**, 3205–3217.
- 56 D. Naumann, W. Tyrra, R. Gnann, D. Pfolk, T. Gilles and K.-F. Tebbe, *Z. Anorg. Allg. Chem.*, 1997, **623**, 1821–1834.
- 57 P. Cortés Soláns, M. L. Bubenik, M. H. Lee, P. S. Riemann and A. Pérez-Bitrián, *Inorg. Chem.*, 2025, **64**, 23184–23191.
- 58 K. Koppe, V. Bilir, H.-J. Frohn, H. P. A. Mercier and G. J. Schrobilgen, *Inorg. Chem.*, 2007, **46**, 9425–9437.
- 59 D. Naumann, W. Tyrra, R. Gnann and D. Pfolk, *J. Chem. Soc., Chem. Commun.*, 1994, 2651.
- 60 D. Naumann and W. Tyrra, *J. Chem. Soc., Chem. Commun.*, 1989, 47–50.
- 61 H. J. Frohn and S. Jakobs, *J. Chem. Soc., Chem. Commun.*, 1989, 625–627.
- 62 H. Böhrer, N. Trapp, D. Himmel, M. Schleep and I. Krossing, *Dalton Trans.*, 2015, **44**, 7489–7499.
- 63 M. Rohde, L. O. Müller, D. Himmel, H. Scherer and I. Krossing, *Chem.–Eur. J.*, 2014, **20**, 1218–1222.
- 64 K. M. Marzenko, H. P. A. Mercier, J. T. Goettel and G. J. Schrobilgen, *Angew. Chem., Int. Ed.*, 2025, **64**, e202425216.
- 65 H.-J. Frohn and V. V. Bardin, *Organometallics*, 2001, **20**, 4750–4762.
- 66 R. Filler, *Isr. J. Chem.*, 1978, **17**, 71–79.
- 67 A. Kraft, J. Beck, G. Steinfeld, H. Scherer, D. Himmel and I. Krossing, *Organometallics*, 2012, **31**, 7485–7491.
- 68 F. Scholz, D. Himmel, L. Eisele, W. Unkrig, A. Martens, P. Schlüter and I. Krossing, *Chem.–Eur. J.*, 2015, **21**, 7489–7502.
- 69 S. Grimme, A. Hansen, S. Ehlert and J.-M. Mewes, *J. Chem. Phys.*, 2021, **154**, 064103.
- 70 (a) CCDC 2529884: Experimental Crystal Structure Determination, 2026, DOI: [10.5517/ccdc.csd.cc2qzk5d](https://doi.org/10.5517/ccdc.csd.cc2qzk5d); (b) CCDC 2529885: Experimental Crystal Structure Determination, 2026, DOI: [10.5517/ccdc.csd.cc2qzk6f](https://doi.org/10.5517/ccdc.csd.cc2qzk6f); (c) CCDC 2529886: Experimental Crystal Structure Determination, 2026, DOI: [10.5517/ccdc.csd.cc2qzk7g](https://doi.org/10.5517/ccdc.csd.cc2qzk7g); (d) CCDC 2531335: Experimental Crystal Structure Determination, 2026, DOI: [10.5517/ccdc.csd.cc2qz1zr](https://doi.org/10.5517/ccdc.csd.cc2qz1zr).

